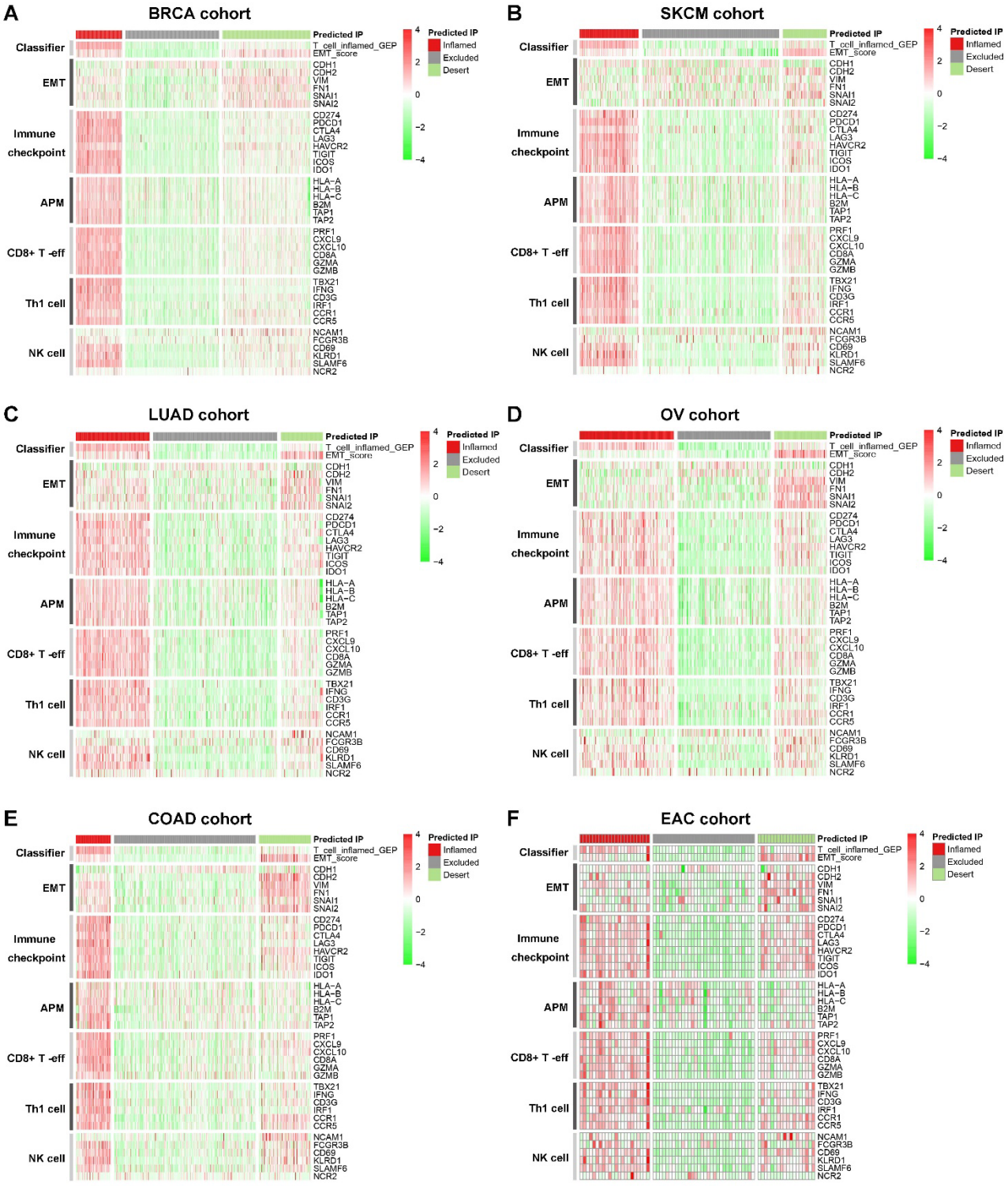

Supplementary Fig. S1. Heatmap of the expression of marker genes in the critical functional gene sets in 6 types of cancer cohorts from TCGA.

The TCGA cancer cohort were stratified as inflamed-type, excluded-type, and desert-type tumors by our predicted immunophenotype (predicted IP). AMP, antigen presenting machinery. (A) Breast cancer (BRCA) cohort. (B) Melanoma (SKCM) cohort. (C) Lung cancer (LUAD) cohort. (D) Ovary cancer (OV) cohort. (E) Colon cancer (COAD) cohort. (F) EAC cancer (EAC) cohort.

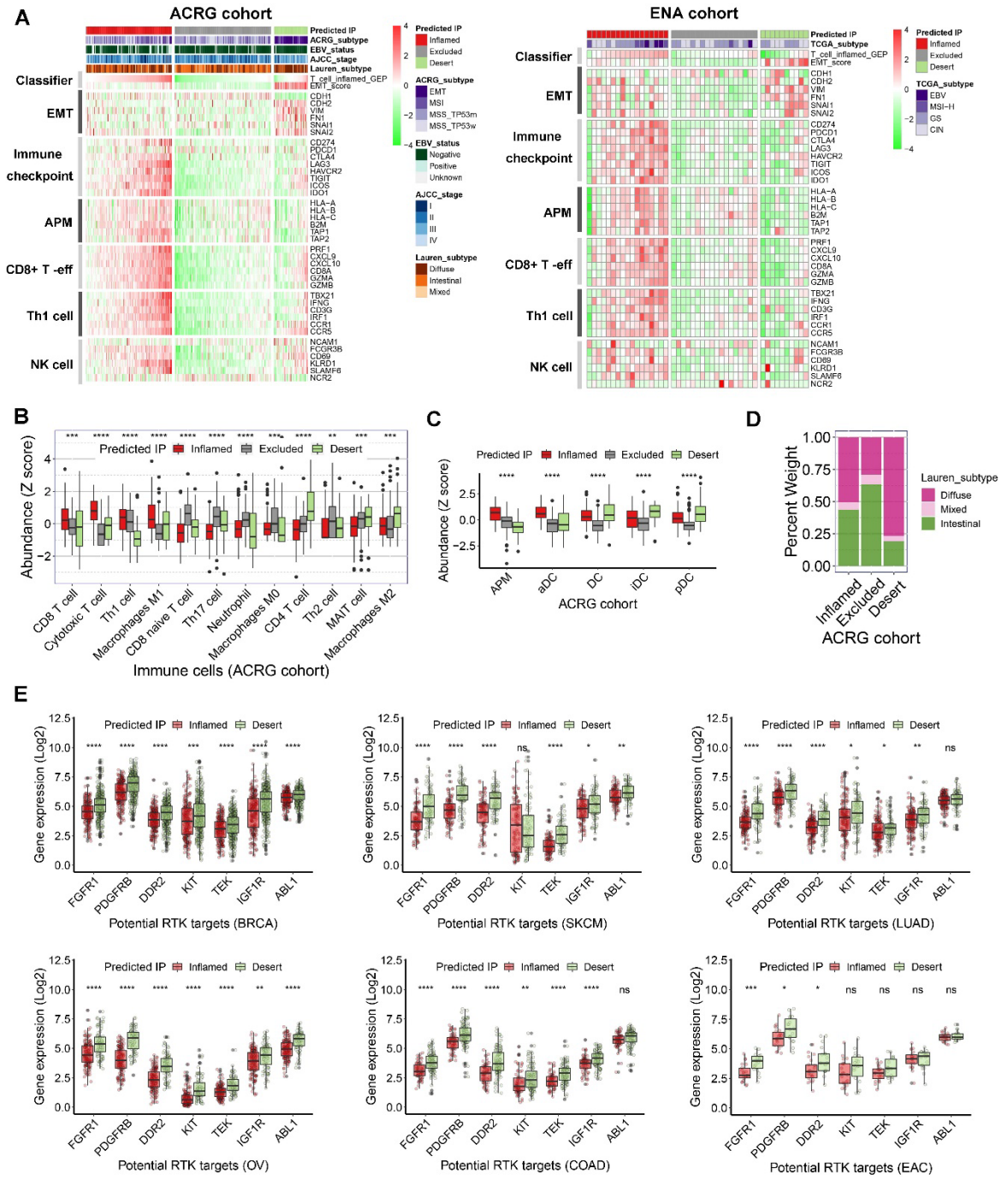

Supplementary Fig. S2. Variation of clinical features, immunotherapeutic response and prognosis among the subtypes of predicted immunophenotype

(A) Heatmap presented the expression of marker genes in several functional gene sets in ACRG and ENA gastric cancer cohorts. (B) The abundance of immune cells valuated by the immune cell abundance identifier (ImmuCellAI) and CIBERSORT tools in ACRG cohort. The values were normalized into z score. (C) The abundance of various population of dendritic cells (DCs) in ACRG cohort. (D) Correlation of predicted immune phenotype (IP) with Lauren subtype in ACRG cohort. (E) The relative mRNA expression of a group of receptor tyrosine kinases (RTKs) in the predicted desert-type tumors, compared to the predicted inflamed-type tumors, in TCGA cohorts from different types of cancer.

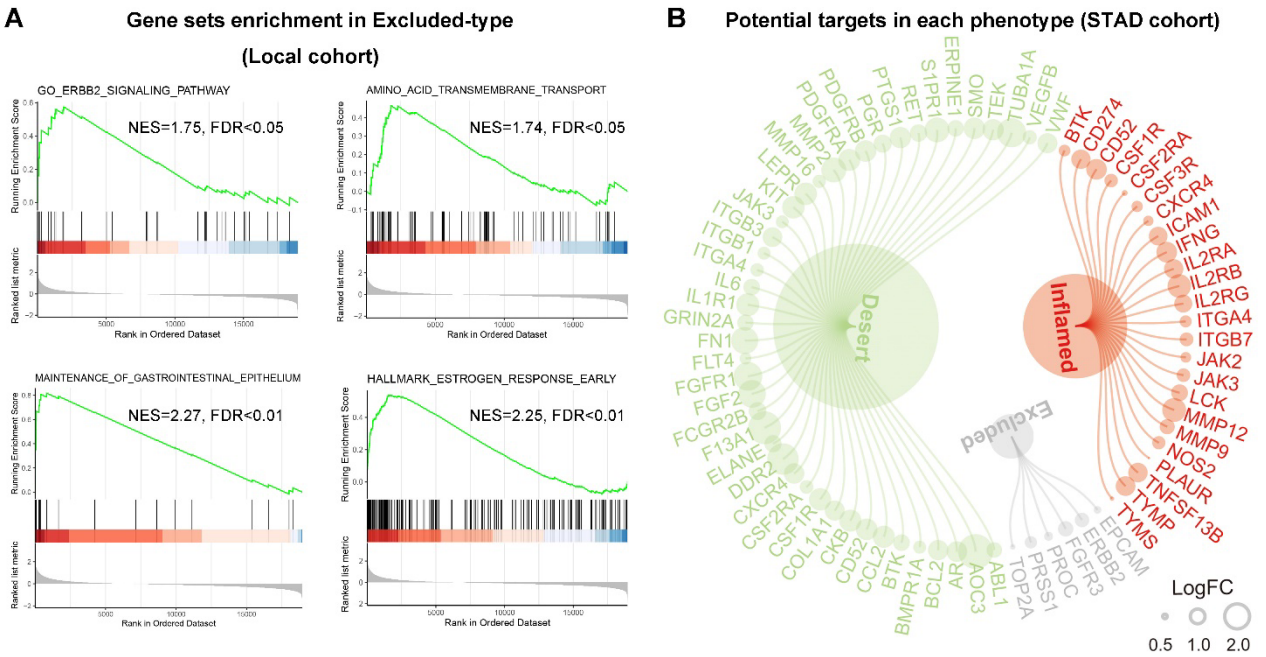

Supplementary Fig. S3. GSEA and potential druggable targets in the immune-excluded type gastric tumors

(A) The top gene signatures were enriched in immune-excluded gastric tumors, such as ERBB2 signaling, amino acid transmembrane transport, gastrointestinal epithelium, and estrogen response. (B) The potential druggable targets in different immunophenotypes in TCGA gastric tumors (STAD cohort) which were stratified by the predicted IP.

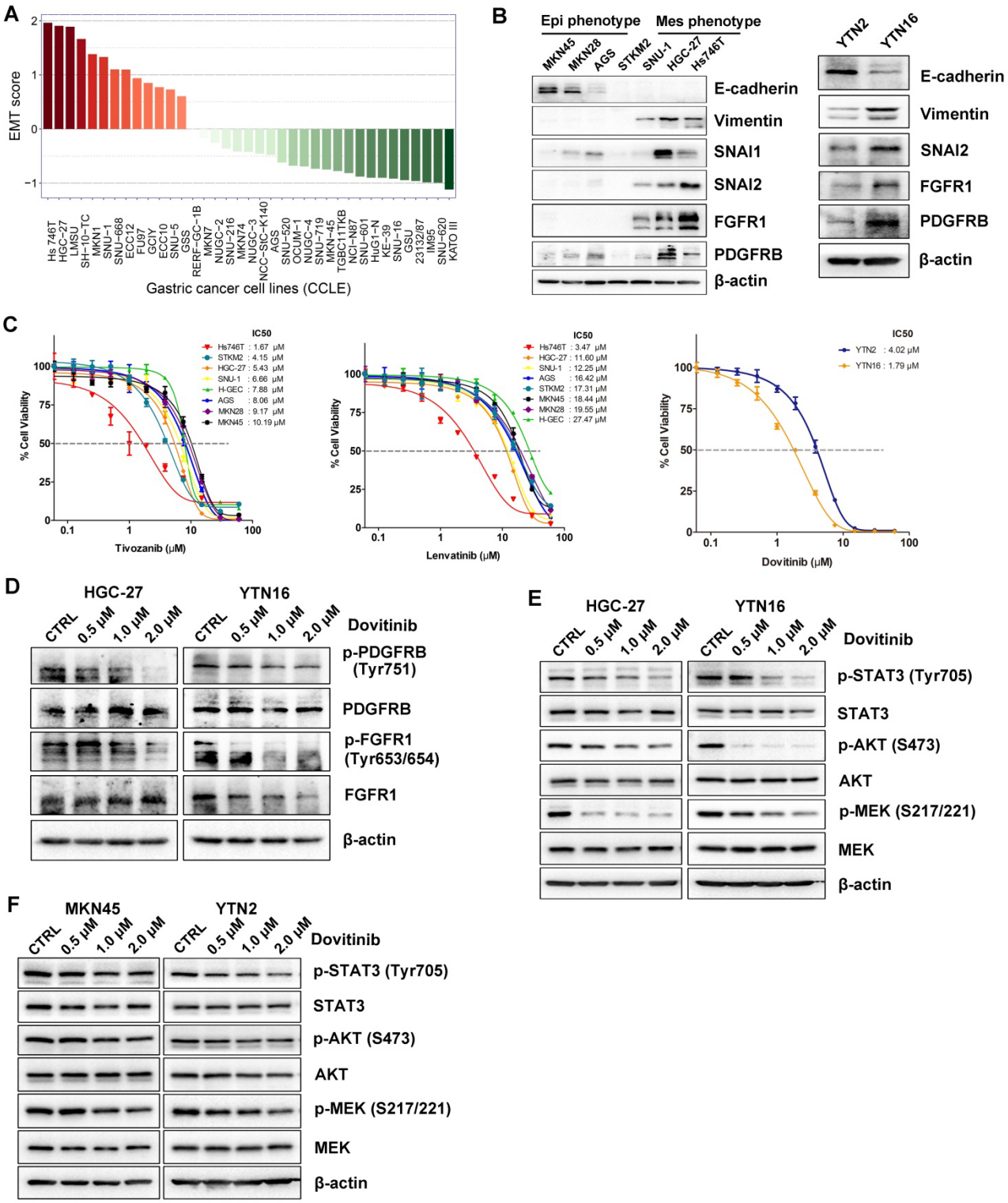

Supplementary Fig. S4. The mesenchymal-like gastric cancer cell lines are sensitive to Dovitinib

(A) EMT scores were calculated in 37 gastric cancer cell lines from Cancer Cell Line Encyclopedia (CCLE) database. (B) Western blots of E-cadherin, Vimentin, SNAI1/2, FGFR1 and PDGFRB in human and mouse gastric cancer cell lines. (C) ATP-Glo cell viability assays of human GC cell lines (Hs 746T, HGC-27, SNU-1, AGS, STKM2, MKN45 and MKN28) and the normal human gastric epithelial cell line (H-GEC) with tivozanib or lenvatinib. The two mouse GC cell lines, epithelial-like type cells (YTN2) and mesenchymal-like

type cells (YTN16), were utilized for ATP-Glo cell viability assay with dovitinib treatment. (D-F) Western blots of PDGFRB, FGFR1 and their downstream targets in human and mouse gastric cancer cell lines.

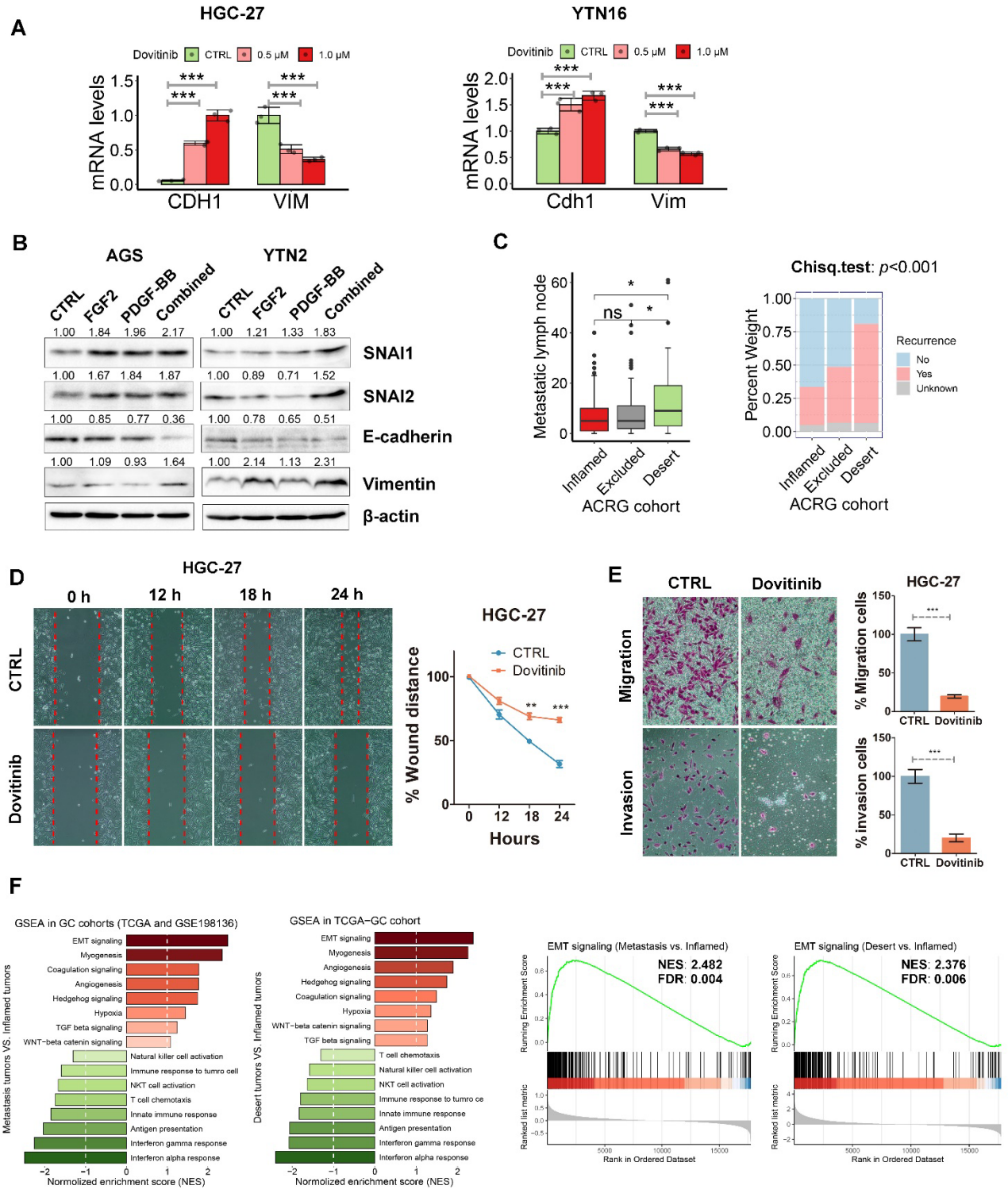

Supplementary Fig. S5. Dovitinib restricts EMT program in mesenchymal gastric cancer cells

(A) qRT-PCR analysis for *CDH1/Cdh1* and *VIM/Vim* expression in HGC-27 or YTN16 cells with indicated doses of dovitinib. CTRL: vehicle control. (B) Western blots of E-cadherin, Vimentin, and SNAI1/2 in AGS and YTN2 cell lines with incubation with FGF2, PDGF-BB, or the combination of these recombinant proteins. The quantification of protein bands were performed by ChemiDoc™ Imaging Systems (Bio-Rad), normalized to β-actin, compared to the control (CTRL). (C) Boxplots of high lymph node metastasis and recurrence in

the desert-type tumors of ACRG cohort. (D and E) Wound healing assays (D), migration and invasion assays (E) were performed in HGC-27 cells after 24 hours 1.0μM dovitinib treatment. The quantification of % wound distance and migration and invasion cells is shown as the mean ± SD of 3 independent experiments (right). **p<0.01, ***p<0.001. (F) GSEA was performed on GSE198136 (21 baseline metastatic gastric tumors) and/or TCGA gastric tumor (GC) cohort. The batch effects between the different datasets were removed before analysis. The desert type and inflamed type tumors in the TCGA-GC cohort were stratified using 'predicted immunophenotype'. GSEA of EMT signaling was shown with normalized enrichment scores (NES) and false discovery rate (FDR).

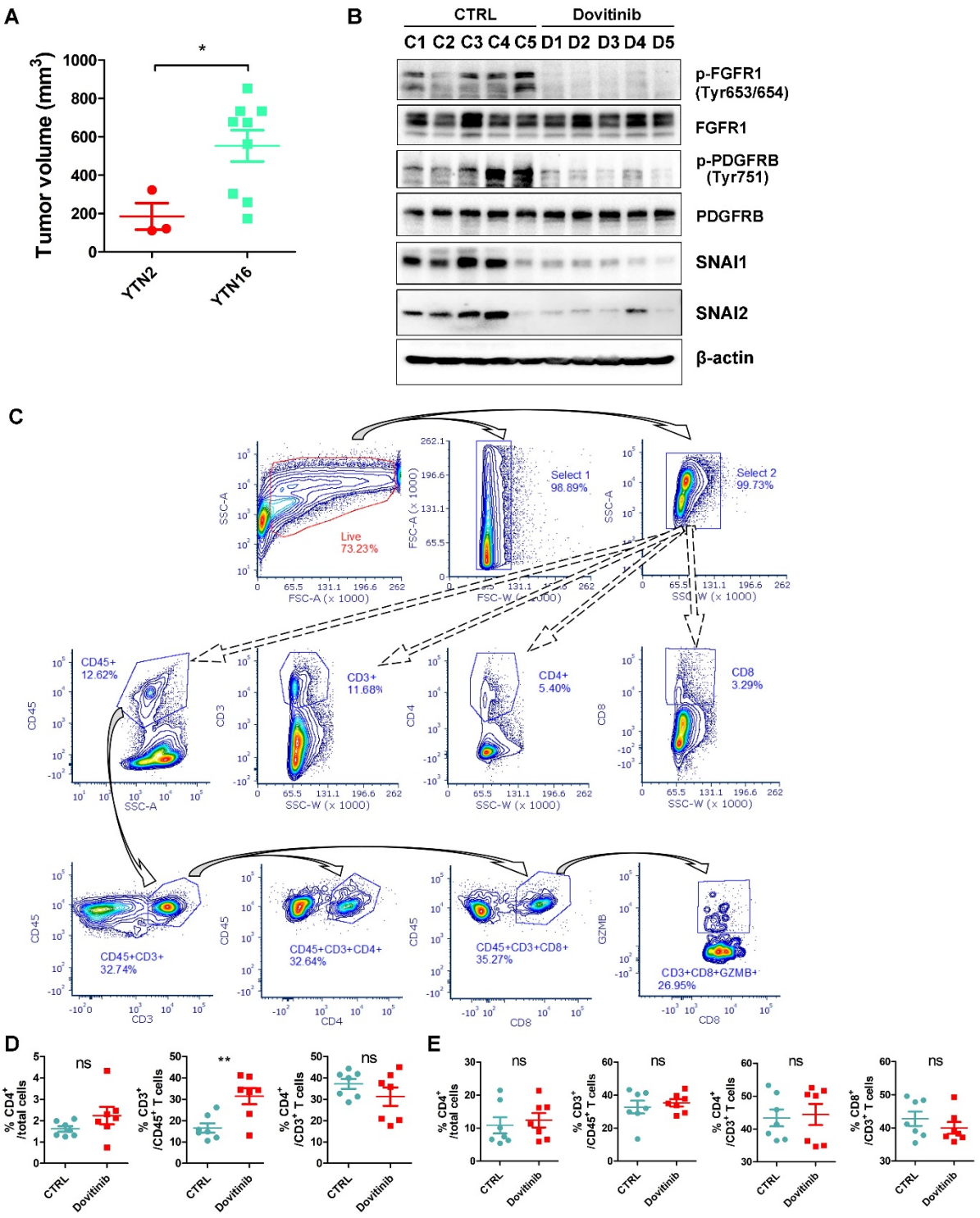

Supplementary Fig. S6. Dovitinib reprograms TME by promoting CD8$^+$ T cell recruitment

(A) Scatter plots of the tumor volumes of YTN2-derived and YTN16-derived syngeneic tumors at 10 weeks post implantation. (B) Western blots for multiple RTKs and its downstream targets of dovitinib-treated syngeneic tumors. (C) Gating strategy used in flow cytometric analysis of CD45/CD3/ CD4/CD8/GZMB from harvested syngeneic tumors. (D and E) Flow cytometry analysis for CD45$^+$/CD3$^+$/ CD4$^+$/CD8$^+$ T cells in the syngeneic tumors (D) and the spleens of relevant tumor-bearing mice (E). ns indicate no significance, *p < 0.05, **p < 0.01.

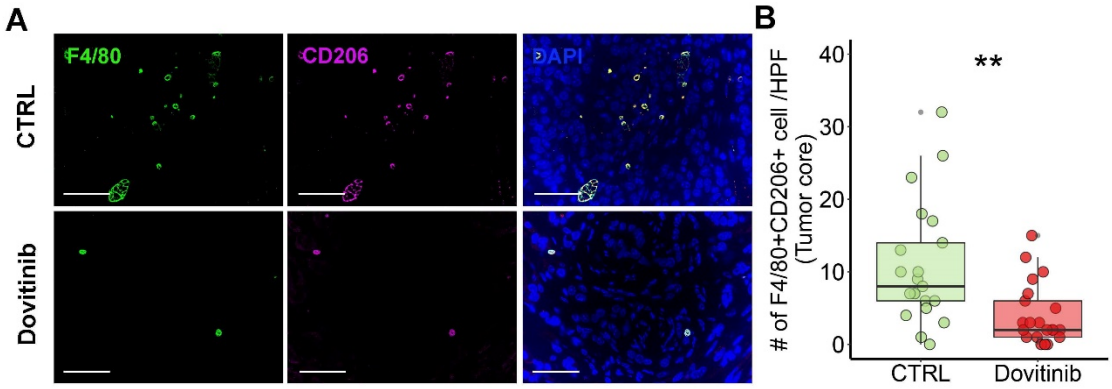

Supplementary Fig. S7. Dovitinib decreases M2-like macrophages in tumors

(A) Representative immunofluorescence staining of F4/80 (green), CD206 (red), and DAPI (blue) in YTN16-derived syngeneic mouse tumor core with dovitinib treatment. (B) The quantification of $F4/80^{+}CD206^{+}$ M2 macrophage cells was shown as 3 independent high-power fields for each tumor. Each group included 7 tumors.

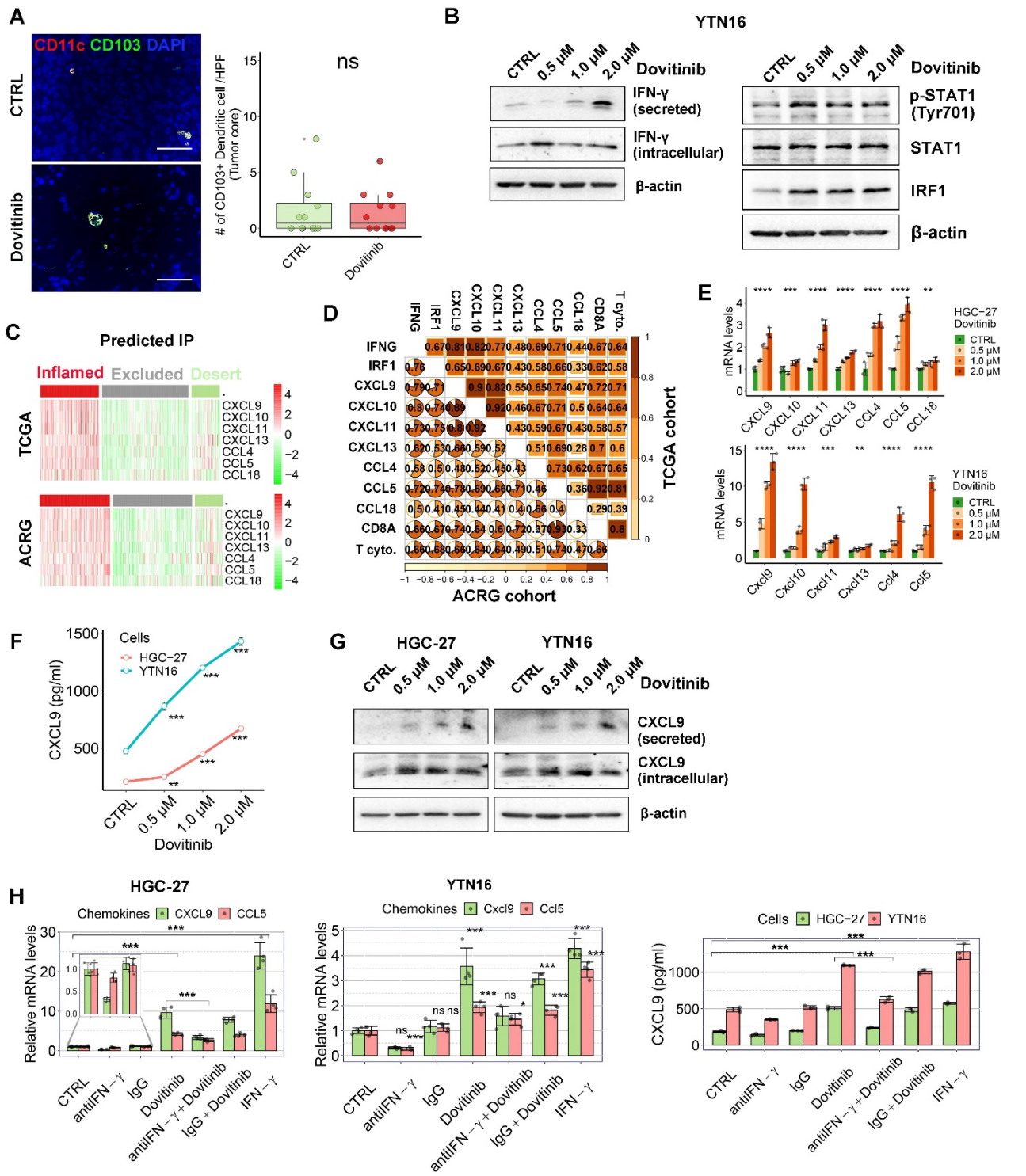

Supplementary Fig. S8. Dovitinib promotes CD8$^+$ T cell infiltration via activation of IFN-γ signaling

(A) Representative images of immunofluorescence staining (scale bars, 50μm) for CD11c (red), CD103 (green) and DAPI (blue) in syngeneic tumors. The quantification of Dendritic cell/HPF is shown as the mean ± SD of 3 independent fields for each staining. ns indicate no significance. Each group included 4 tumors. (B) Western blots of p-STAT1 (Tyr701), STAT1 and IRF1 in YTN16 cells with 24 hours treatment of indicated doses of dovitinib. (C) Heatmap of a group of overexpressed chemokines in the predicted inflamed-type tumors, compared to the predicted desert-type tumors in TCGA and ACRG cohorts. (D) Pearson's correlation analyses

of the chemokines from (C) and cytotoxic T cell infiltration signature. (E-G) qRT-PCR analysis of the chemokines (E), ELISA of CXCL9 in the medium (F), and Western blots of CXCL9 (G) in HGC-27 or YTN16 cells treated with dovitinib. (H) HGC-27 or YTN16 cells were incubated with IFN-γ neutralization antibody and treated with dovitinib as indicated. CTRL: vehicle control. IgG and recombinant IFN-γ work as controls. qRT-PCR analysis of *CXCL9(Cxcl9)*/*CCL5(Ccl5)* (left and middle) and ELISA of human CXCL9 in HGC-27 cells and mouse CXCL9 in YTN16 cells (right) in the neutralization experiments. ns indicate no significance, *p < 0.05, **p < 0.01. ***p < 0.001.

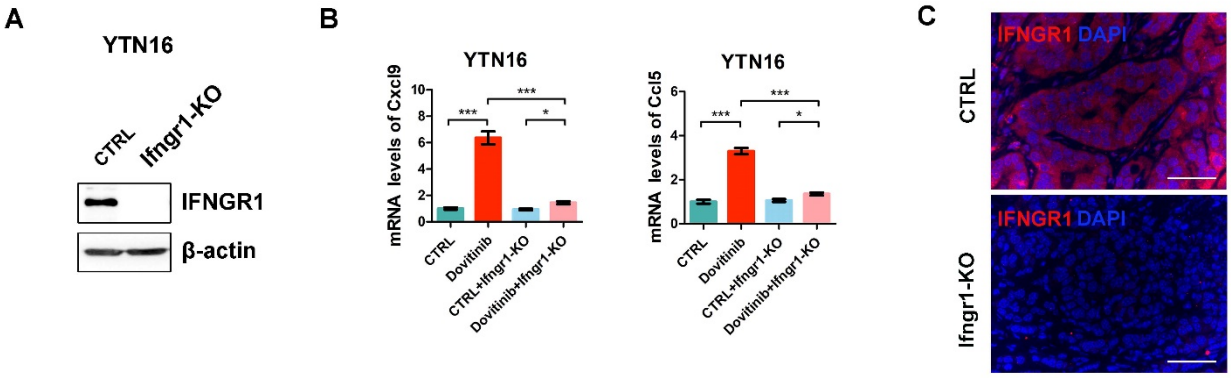

Supplementary Fig. S9. Dovitinib transcriptionally upregulates *Cxcl9* and *Ccl5* expression depending on tumor intrinsic IFN-γ/IFNGR1 signaling axis

(A) Western blots of IFNGR1 in YTN16 cells with *Ifngr1* knockout (KO). CTRL: parental cells. (B) qRT-PCR analysis showed the expression of *Cxcl9*/*Ccl5* in YTN16 cells with dovitinib treatment and/or *Ifngr1* knockout. (C) Representative images of immunofluorescence staining (scale bars, 50μm) of IFNGR1 (red) expression in syngeneic tumors derived from YTN16 cells (CTRL) or YTN16 cells with *Ifngr1*-KO.

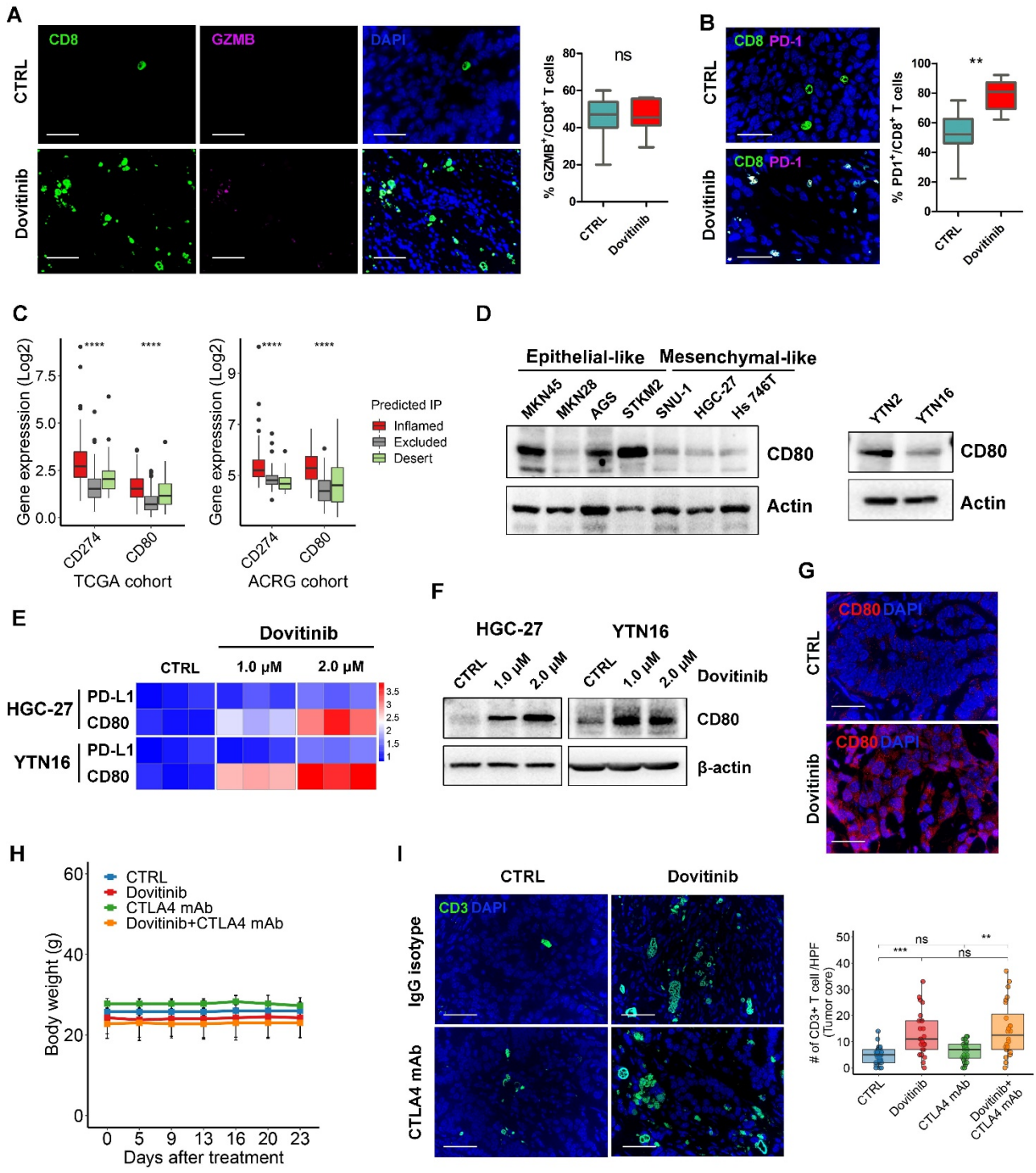

Supplementary Fig. S10. Targeting multiple RTKs synergizes with CTLA4 blockade to potentiate anti-tumor immunity

(A - B) Representative images of immunofluorescence staining (scale bars, 50μm) for CD8/GZMB//DAPI (A) or CD8/PD-1 (B) in YTN16-derived syngeneic tumors treated with dovitinib or the vehicle control. The quantification of $CD8^+$ T cell/HPF is shown as the mean ± SD of 3 independent fields for each staining. Each group included 7 tumors. (C) Relative mRNA expression of *CD274* and *CD80* in the predicted immunophenotypes of TCGA and ACRG cohorts. (D) Western blots of CD80 in GC cell lines. (E) Heatmap of

qPCR analysis of *PD-L1(CD274)* and *CD80* in HGC-27 and YTN16 cells treated with indicated doses of dovitinib. (F) Western blots of CD80 in HGC-27 and YTN16 cells with dovitinib treatment. (G) Immunofluorescence staining (scale bars, 50μm) for CD80/DAPI in the syngeneic tumors treated with dovitinib, or the vehicle control. (H) Plots of mice body weight of C57BL/6 mice implanted with YTN16 cells treated with dovitinib, CTLA-4 mAb or the combination. Each group included 6 mice. (I) Immunofluorescence staining (scale bars, 50μm) for CD3/DAPI (H) in the syngeneic tumors treated with CTLA4 mAb or IgG control. The quantification of $CD3^+$ T cell/HPF is shown as the mean ± SD of 3 independent fields for each staining (right). Each group included 8 tumors. ns indicates no significance, **p < 0.01, ***p < 0.001.